Analysis of Coupled CFD-DEM Simulations in Dense Particle-Laden Turbulent Jet Flow

Conference Paper · October 2020

DOI: 10.1115/FEDSM2020-20274

2 authors:

Dustin Weaver
University of British Columbia - Okanagan
6 PUBLICATIONS **38** CITATIONS
SEE PROFILE

Sanja Miskovic
University of British Columbia
30 PUBLICATIONS **309** CITATIONS
SEE PROFILE

Proceedings of the ASME 2020 Fluids Engineering Division Summer Meeting
FEDSM2020
July 12-16, 2020, Orlando, Florida, USA

FEDSM2020-20274

ANALYSIS OF COUPLED CFD-DEM SIMULATIONS IN DENSE PARTICLE-LADEN TURBULENT JET FLOW

Dustin Weaver
Department of Mining Engineering
University of British Columbia
Vancouver, British Columbia
Canada
d.weaver@alumni.ubc.ca

Sanja Miskovic
Department of Mining Engineering
University of British Columbia
Vancouver, British Columbia
Canada
sanja.miskovic@ubc.ca

ABSTRACT

In this paper, coupled CFD-DEM simulations of dense particle-laden jet flow are performed using CFDEM® coupling interface that couples LAMMPS-based LIGGGHTS® DEM engine with OpenFOAM CFD framework. Suspensions of mono-sized spherical glass particles with 80 microns diameter and a mass loading of 0.23 and 0.86 are considered. Three different CFD meshes are used with an average mesh resolution dimension of 3.06, 2.67, and 1.86 particle diameters and it is determined that mesh resolution does not change results for void fraction calculation (using the divided model) of the CFD-DEM equations. Samples of particle flux are taken at 0.1, 10, and 20 nozzle diameters along the axial direction of the jet region. The numerical results for particle flux are compared with a well cited experimental data found in literature. The CFD-DEM simulations in turbulent jet flow are found to be highly sensitive to initial particle velocity inputs but the experimental data provide sufficient information to produce comparable results.

NOMENCLATURE

- α void fraction
- ρ density
- u velocity
- p pressure
- τ stress tensor
- K coupling implicit momentum source term
- f explicit momentum forcing term
- F generic particle force
- V volume
- I moment of inertia of the particle
- ω angular velocity
- T torque acting on the particle
- L characteristic length
- G particle flux (number of particles per second per area of measurement) where Gm is max particle flux
- d particle diameter
- D nozzle diameter
- r radial distance from the jet center

INTRODUCTION

Two or three phase particle-laden jet flows are relevant to a wide range of engineering and science applications including jet mills, abrasive jet machining, locomotive sanding, surface coating, among many others. To optimize the equipment in these applications, advanced numerical techniques can be used to facilitate design improvements and optimize unit operation. Accuracy of these models depends on the correct simulation parameters that require a fundamental understanding of the numerical method and its application. Much research has been performed experimentally for turbulence dense particle-laden jet flow with a variety of Reynolds numbers [1–8], but from the author's knowledge a numerical analysis of fully turbulent dense jet flow using CFD-DEM approach is limited in literature [9]. The aim of the current research is to apply the CFD-DEM technique to simulate

dense turbulent jet flow and analyze its accuracy and ability in capturing flow details.

CFD-DEM coupled simulations can be classified by the use of a resolved or unresolved method. Resolved methods use an "immersed boundary" method that requires the CFD mesh size to be at least 10 times the particle size [10]. This method is restricted to simulations that consider very few particles and is not practical in many applications. For non-dilute particle-laden flow, an unresolved approach can be used, where the fraction of particles is first calculated in each cell (solids void fraction). The void fraction is then used in tandem with averaged particle properties to calculate the momentum exchanges between the two phases. The methods of void fraction estimation produce a source of error in simulations when the particle size is approaching the size of the cell. Therefore, an issue arises when determining a sufficiently refined grid size for accurate modeling of the fluid flow, while also allowing an accurate representation of the physics of large particles. In the present research, three average mesh size dimensions of 3.06, 2.67, and 1.86 particle diameters are used to determine if there are any discrepancy or errors in void fraction calculation. The goal of the present research is to make a comparison of CFD-DEM simulations to experimental data while also determining a mesh size resolution for the given particle diameter that allows a sufficiently fine mesh for fluid flow with the ability to add larger particles. Although the particles in the present study are small (80 microns), the observed trends in mesh resolution relative to the particle size are intended to be used when there is a desire to consider larger particles in future work.

EXPERIMENT

Apparatus

The experimental data used to validate the model in the current study is given by Hardalupas et. al. [4]. The paper is well cited (150+) in the field of turbulent particle-laden jets and was chosen for its thorough analysis of input and output particle flux and velocity fluctuations for particles of sizes 40, 80, and 200 microns. Simulating 40 micron particles using CFD-DEM method is questionable because the volume of a 40 micron particle is very close to machine zero and, hence, the accuracy is compromised. Authors do not provide the particle flux profiles for the 200 micron particles, so the focus of the present study is on the analysis of flows with 80 micron particles. The experimental setup is a jet configuration with supporting instrumentation for flow control and measurement that is shown in Fig. 1.

The particles are mixed with the free stream air in a chamber just above the nozzle. The particle-laden flow then moves from the chamber to a smooth bore stainless steel tube with 15 mm diameter (D). The length of the nozzle is 66 nozzle diameters to ensure that the flow is fully developed at the exit of the nozzle. Results are collected along the axial direction of the jet at 10 and 20 nozzle diameters from the nozzle exit by a Phase-Doppler anemometer. The bulk velocity at the exit of the flow is kept at a constant 15 $\mathrm{m\,s^{-1}}$ corresponding to a Reynolds number of 13000. The reader is encouraged to read Hardalupas et al., 1989 for an in-depth discussion of the experiment [4].

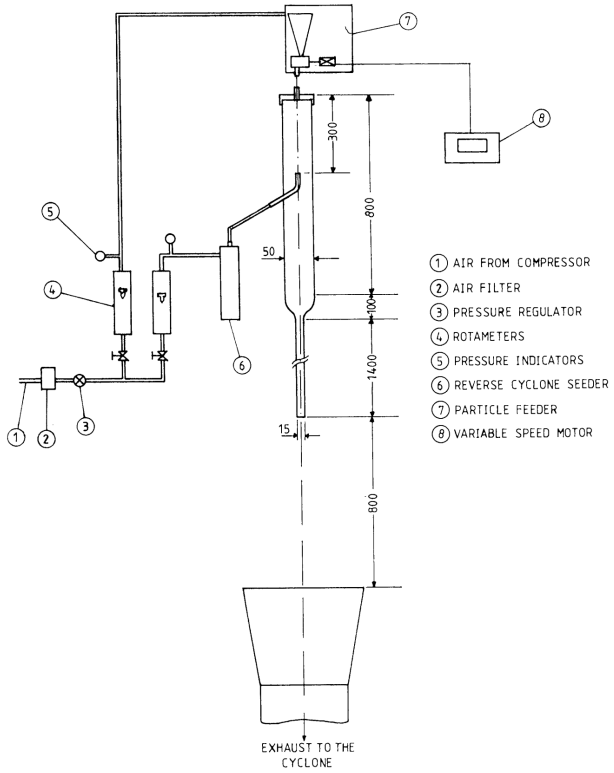

FIGURE 1. EXPERIMENTAL APPARATUS USED BY HARDALUPAS ET AL. [4]

Material

Mass loading, which is defined as a ratio of the mass fluxes of two phases, of 0.23 and 0.86 is used for all experiments. These values are chosen to ensure a significant contribution of particle momentum onto the fluid, while also attempting to reduce the effect of particle-particle collisions. Determination of the material properties of the solids has proven to be challenging. In the given experiment, the 80 micron glass beads are said to have a molecular film of silicone material used to prevent agglomeration, but no other information about the material properties was given. Therefore, an educated assumption is made that the behavior of the particles closely matches the properties of pure glass beads. In Lorenze et al. [11], the coefficient of restitution for glass on smooth aluminum plate is 0.816, with a coefficient of friction of 0.131. A Poisson's ratio of 0.3 with the very low rolling friction coefficient of 0.01 is also assumed, which are the values that are used in the present numerical simulations.

It should be noted here that accurate inputs into any CFD-DEM model are of high importance. If the experiments and parameters used to validate and expand these models are not comprehensive enough, a researcher must make assumptions that could otherwise be avoided. That being said, the coefficients of friction and restitution are not of high significance in the present study because the volume fraction of particles is sufficiently low and, therefore, the only critical consideration is the collision coefficient for the particles along the wall region and not particle-particle interactions. For these reasons, we believe that the accuracy of the developed model and obtained results are reasonable enough.

NUMERICAL MODEL

The fluid phase of the coupled CFD-DEM model is described by the Navier-Stokes equations, with an added source term to account for the momentum of the solid-phase. The incompressible Navier-Stokes equations are given by:

$$\nabla \left(\alpha_f \rho_f u_f\right) = 0 \tag{1}$$

$$\begin{aligned}\nabla \cdot \left(\rho_f \alpha_f \vec{u}_f \vec{u}_f\right) = &- \alpha_f \nabla p + \nabla \cdot \left(\alpha_f \tau_f\right) - K_{sf}\left(\vec{u}_f - \vec{u}_s\right) \\ &+ \alpha_{/} f \rho_f \vec{g} + f\end{aligned} \tag{2}$$

where, α_f is the fluid phase volume fraction, $\vec{u}_f$ is the fluid velocity, $\vec{u}_s$ is the mean solid particle velocity, τ_f is the fluid phase stress tensor, and K_{sf} is the implicit momentum source term that is a volume average of all interacting forces acting on the solid phase due to the motion of the fluid in each cell [12]. It is given by:

$$K_{sf} = \frac{\alpha_f \sum\limits_i \bar{F}_d}{V_{cell} \cdot \left|\vec{u}_f - \vec{u}_p\right|} \tag{3}$$

The fluid phase volume fraction, or void fraction, α_f, is directly linked to the carrier phase momentum and, therefore, is a critical parameter to consider in these coupled simulations. The void fraction is the measure of the particle volume fraction inside of each cell. It is possible to calculate this volume exactly, but the approach is computationally costly, and instead, a simplified model is used. The centered method is the simplest model that assumes the entire particle volume is located in the center of the particle and, as a consequence, a considerable portion of the particle could be located outside of the cell. This method is efficient but inaccurate, even with particles that are an order of magnitude smaller than the cell size.

The divided void fraction model uses a different approach that approximates the particle volume by "dividing" the particle into separate regions that are then spread across multiple cells. In CFDEM®coupling, the volume is divided into 29 non-overlapping regions of equal volume. The centroid of each region, or volume, is then used to determine the respective cell in which the new region exists, and the void fraction is then calculated. The void fraction used in all of these simulations is the divided model. More information about the model and its implementation is given in the CFDEM®coupling user guide [13].

Turbulence is modeled by Reynolds averaging of Eqn. 1 and Eqn. 2 (RANS). These equations are subsequently closed by the two equation turbulence model $k\omega - SST$. The default coefficients are adopted in the model with the equations listed in the OpenFOAM user guide [14]. OpenFOAM uses an updated version of the base $k\omega - SST$, which is given by Menter et al. [15], and was not modified from this implementation. For more details about these models and their implementation, the reader is referred to the OpenFOAM user guide [14] and the paper by Menter et al. [15].

A wall function based on Spalding's law is used to model the boundary layer. This formula models the entire range of boundary layer [16]. The use of the wall function is important in the present study because mesh refinement puts the y+ value across different sections of the boundary layer.

The translational and rotational velocity for particles are given by Newton's 2nd law

$$\begin{aligned}m_p \frac{du_p}{dt} = &- u_p \nabla p + F_{drag} + m_p g + F_{visc} \\ &+ \sum_{N_p} F_{p-p} + \sum_{N_p} F_{p-w}\end{aligned} \tag{4}$$

$$I_p \frac{d\omega_p}{dt} = T_p \tag{5}$$

where, going from the left to the right in Eqn. 4 we have pressure, drag, gravitational, viscous, particle to particle, and particle to wall forces. The F_{drag} in the present research is calculated by the drag model proposed by Koch and Hill (2001) [17]. Further information about the full coupled equations implemented into CFDEM®coupling can be found in the paper by Buijetenen et al. [18].

SIMULATION SETUP

The open-source software CFDEM®coupling used in the present study couples OpenFOAM CFD toolbox with LIGGGHTS DEM code.

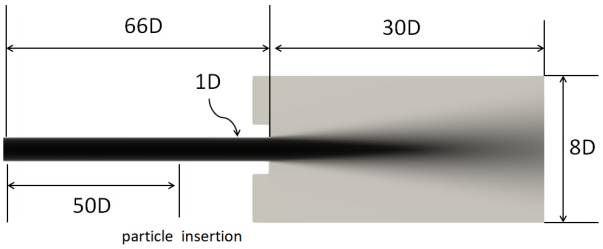

FIGURE 2. CFD DOMAIN SLICE WITH MAIN DIMENSIONS; 1D = 15mm

CFD Model Setup

A three-dimensional domain is considered with a nozzle diameter of 15 mm and nozzle length equivalent to 66 nozzle diameters (66D). An axial cross section through the domain with its main dimensions is given in Fig. 2. The long nozzle length is used to ensure that the carrier phase flow field is fully developed by the end of the nozzle, or nozzle outlet. A constant velocity boundary condition of 15 $\mathrm{m\,s^{-1}}$ that produces a Reynolds number of 14678 is defined at the inlet, while a pressure boundary condition set to zero is chosen at the outlet. Turbulent kinetic energy, k, is calculated at the inlet from the traditional formula with turbulent intensity and length scale. A wall function based on Spalding's law is used for the turbulent viscosity [16]. OpenFOAM default ω wall function is also used.

Discretization is done using hexahedral meshes of 1.4, 2.2, and 4.4 million cells. These meshes were produced in Trelis® meshing software. Care was taken to ensure that the mesh skewness was below 0.5, orthogonally less than 30, and shape factor (3/weighted_jacobian) greater than 0.4. A first order implicit scheme is used for temporal discretization. A hybrid second/first order approach is used for spatial discretization. This scheme is second order by default, but limits to first order when there is an extremely large gradient. A pressure-based transient PISO (pressure-implicit split-operator) algorithm proposed by Issa et al. [19] is used for the fluid phase solver. This method has been widely used in CFD since the original paper's publication. Linear solvers are used for velocities, pressure, and all other scalar and vector fields with a pre-conditioner for pressure that uses a multi-grid method. Final solver tolerance is set to 1E^{-8} for all fields.

There is a variability in the cell size of the mesh and, therefore, to quantify the particle to cell size ratio, a pronto specific characteristic length is calculated by the volume of the cell divided by two times the gradient of the volume as given here:

$$L_{pronto} = \frac{V_{cell}}{2\nabla V_{cell}} \tag{6}$$

The average value of Eqn. 6 for the entire mesh is then taken and divided by the particle diameter to obtain the relation for the cell size and particle diameter. The obtained results of characteristic length for the three considered mesh resolutions are: 3.075d for 1.4 million mesh, 2.63d for 2.2 million mesh, and 1.87d for 4.4 million mesh. The "d" in this application denotes the diameter of the particle.

DEM Model Setup

Unless otherwise stated, the inputs into the DEM model are kept the same for all cases. Solids are mono-sized spherical particles with 80 micron diameter and density of 2950 $\mathrm{kg\,m^{-3}}$. Two solids mass loading (fraction of mass flux), namely 0.23 and 0.86, are considered in this work. The reference paper with the experimental data includes data for velocity fluctuations with approximate average values of u',v',w' = 0.4 $\mathrm{m\,s^{-1}}$. A Gaussian distribution of particle velocities is used with a mean velocity of $\vec{u}_p = (13,0,0)$ and standard deviations of 0.4 in all directions. Coefficient of restitution is set to 0.816 and coefficient of friction to 0.131. The values are selected based on the described glass beads given in the experiment. Particles are inserted inside of the nozzle 50D from the CFD inlet. This location was chosen to ensure that the fluid flow was fully developed before particle insertion. The default non-linear Hertzian contact model is used for particle collisions [20]. A time step of 1E^{-6} is chosen for the DEM time-step to ensure that the collisions of particles are fully resolved under the criteria that this time-step is less than 20% of the Rayleigh and Hertzian critical time-steps [21].

CFD-DEM Coupling

The CFD-DEM simulation is coupled in an implicit fashion. The particle forces are calculated from the fluid solution to the Navier-Stokes on the following time step. This implicit way of coupling is very stable for dense flows, but it does go against Newton's third law. This method was chosen because of the ease of implementation in CFDEM®coupling, and explicit coupling will be explored in the future. Koch Hill 2001 [17] model is used for the drag force. This drag force is based off of the lattice Boltzmann equations rather than on experimental data. A particle-based pressure force is applied to the particles and a viscous force is used for fluid-particle interactions. This viscous force is calculated by taking the gradient of τ (the turbulent stress tensor). The CFD time step of 1E^{-5} is chosen with a coupling interval of 10 - the DEM time step performs ten iterations for a single CFD iteration. This is possible because the higher CFD time step still allows fully resolved fluid flow (Courant number less than 0.5), while also conserving the fluid property averaging in each cell.

RESULTS AND DISCUSSION

The simulations are initiated using purely the carrier phase for 0.25 seconds to ensure that the fluid domain is at a pseudo steady-state of fully developed pipe flow. Fluid velocity profiles at the fully developed region are found to compare well to the 1/7 power law. Fig. 3 shows that the fluid flow solution is independent of the mesh resolution with an additional coarse mesh (4.4d) shown for demonstrative purposes. It should be noted that the velocity is also sampled at locations equivalent to 0.1D and 10D from the nozzle outlet and the results consistently demonstrate mesh independence for the fluid flow field.

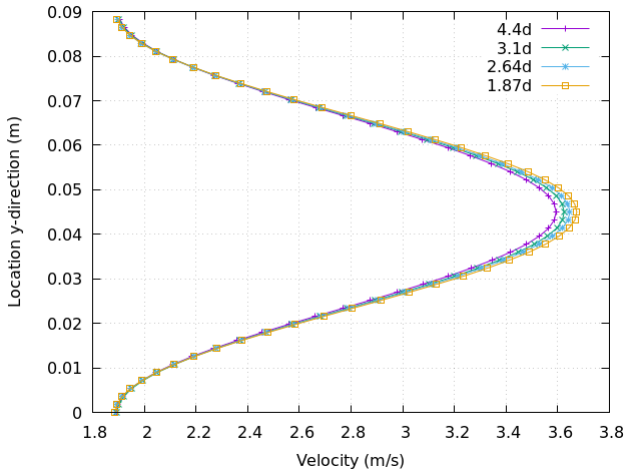

FIGURE 3. FLUID VELOCITY PROFILES FOR DIFFERENT MESH SIZES AT 20 NOZZLE DIAMETERS FROM THE NOZZLE OUTLET

After simulations have reached 0.25 seconds, particles are inserted into the system at a mass loading of 0.23 and 0.86. Particle flux is sampled at 0.1D, 10D, and 20D from the exit of the nozzle. It is observed that there is little to no change in mass flux profiles with a change in mesh resolution as shown in Figure 6. All planes of interest (0.1D, 10D, and 20D) demonstrate the same behavior. It can be concluded that the divided void fraction model in CFDEM®coupling is dividing the volume of particles consistently and that a mesh resolution down to 1.87d can be used with a mass loading up to 0.86 and Reynolds number of 14678.

Figs. 5, 6, & 7 show the particle flux profiles sampled at 0.1D, 10D, and 20D axial distance from the nozzle outlet where *Gm* is the maximum particle flux. The numerical results agree well with the experimental data at 10D and 20D, but do not at 1D. The discrepancy in results at 0.1D could be related to the issues associated with the experimental sampling near the nozzle inlet, discrepancy between input parameters of numerical models

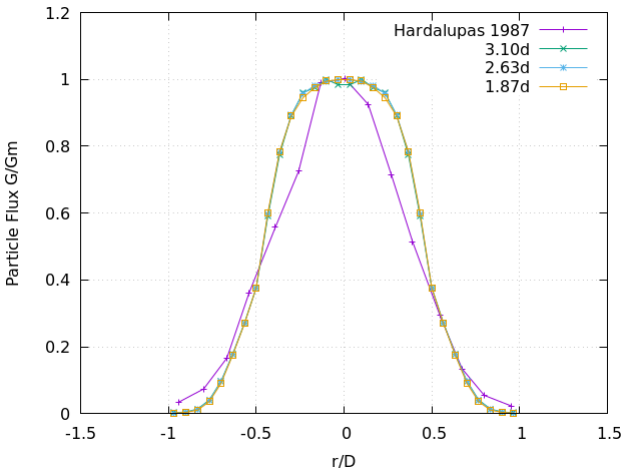

FIGURE 4. PARTICLE FLUX PROFILES FOR 0.23 MASS LOADING AT 10 NOZZLE DIAMETERS FROM THE NOZZLE OUTLET

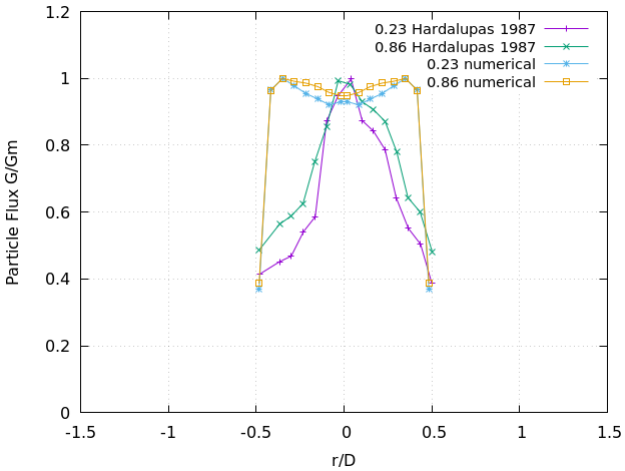

FIGURE 5. PARTICLE FLUX PROFILES WITH A CHANGE IN MASS LOADING AT 0.1 NOZZLE DIAMETERS FROM THE NOZZLE OUTLET

and experiments, and validity of CFD-DEM method for these class of flow problems. Nozzle jet flow is fundamentally a pipe flow that exits into the freestream air. It is, therefore, prudent to discuss the data found in literature on particle-laden pipe flow for an understanding of the almost constant particle flux across the radial direction of the jet directly at the nozzle/pipe exit for the numerical results.

Assuming that the radial particle concentration profiles inside of a turbulent pipe directly relates to the particle flux at a nozzle exit, experimental data from particle-laden flow in pipe applications suggest a variety of behaviors for the shape of radial particle concentration. Shokri et al. [22] observed an almost

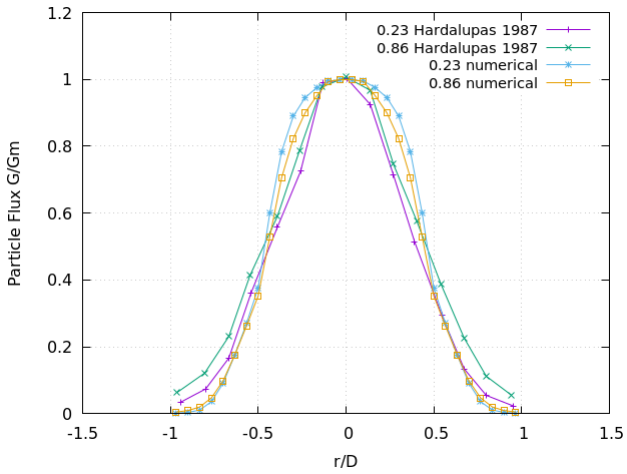

FIGURE 6. PARTICLE FLUX PROFILES WITH A CHANGE IN MASS LOADING AT 10 NOZZLE DIAMETERS FROM THE NOZZLE OUTLET

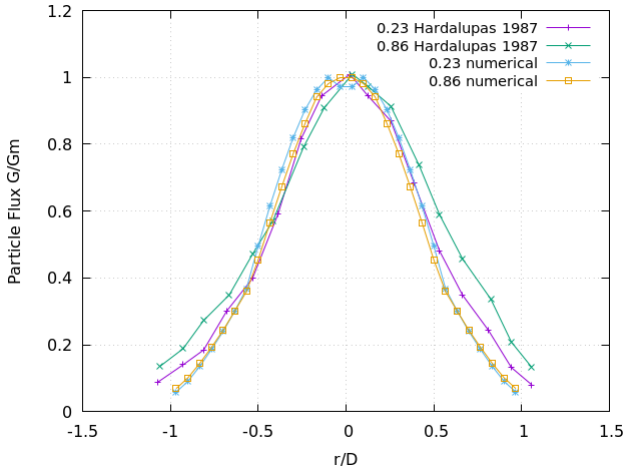

FIGURE 7. PARTICLE FLUX PROFILES WITH A CHANGE IN MASS LOADING AT 20 NOZZLE DIAMETERS FROM THE NOZZLE OUTLET

constant solids concentration profile across the pipe radius with concentration decreasing drastically towards the wall for 0.5 and 1 mm particles and dilute suspension at a Reynolds number of 320000. Most similar to the operating parameters of the experimental data used in the present analysis, Varaskin et al. [23] performed a study using laser Doppler anemometry (LDA) for particle-laden turbulent pipe flow with 50 micron, 2550 $\mathrm{kg\,m^{-3}}$ spherical glass particles at a Reynolds number of 15300 (current study is 14677) with a mass concentration of up to 0.55. The results show that the particle concentration has a uniform distribution across the radial direction of the pipe and tend to that distribution with a sufficient entry length. Similar trends are found in other works [24–26]. In contrast to this, a study performed by Oliveria et al. [27] demonstrates a "coning" of particle concentrations, which is similar to that shown as the experimental data in Fig. 5. It is agreed throughout the literature that the shape of radial concentration profile changes with Reynolds number, particle and fluid properties, and the entry length of the pipe.

The studies considering the affect of entrance length on particle concentration profiles in nozzle flow applications are limited. Lau and Nathan [28] investigated this effect and determined that behavior of particles leaving the jet is similar to that found in the present study shown in Fig. 5. Figures 6 & 7 show very good agreement with the experimental results and, therefore, it is difficult to assign the discrepancy of results at 0.1D as issues could be associated with the numerical model or uncertainty in experimental measurement due to constrained measurement practices near the nozzle exit.

In addition to the experimental considerations addressed above, it is important to discuss a few other critical points relevant to the numerical model accuracy. There is a complex relationship between turbulence of the fluid field and forces on the particles. A viscous force is applied to the particles in the CFD-DEM equations that is defined by:

$$F_{visc} = -\nabla\tau \tag{7}$$

where, τ is the deviatoric stress tensor in the Navier-Stokes equations. The stress tensor can be thought of as the contribution of turbulence onto the momentum of the fluid and, therefore, with a high gradient of turbulence a greater force is applied to the particles. Figure 8 shows the turbulent kinetic energy calculated from the flow field. As the flow exits the nozzle, a high amount of turbulence is produced from the momentum exchange between the jet and the freestream. The viscous force is applied to the particles at this location and pushes the particles towards the outer regions of the jet.

By using the Boussinesq hypothesis with the $k\omega - SST$ turbulence model to close the fluid flow equations in the simulations, the deviatoric stress tensor is considered proportional to the mean rate of strain of the fluid and modelled by an effective viscosity applied to the fluid flow field. The use of effective viscosity assumes isotropic turbulence. This is a good assumption for many applications, but separating flows tend to have anisoptropic turbulence that can only be captured by methods such as LES and DNS, which can fully capture the turbulent eddies in the far field. In the present application, there could be a significant portion of anisotropic turbulence (depending on the Reynolds number) as the boundary layer separates when leaving the nozzle and it is important to capture this behavior so that the correct forces are being applied to the particles. It is therefore important to con-

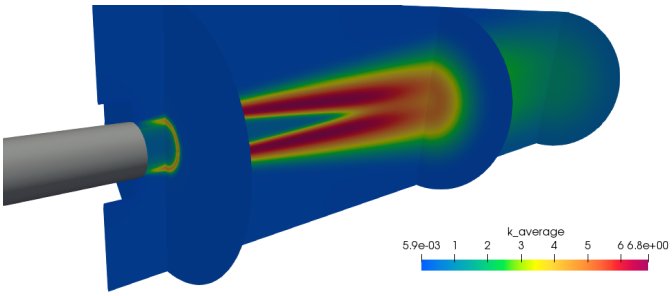

FIGURE 8. AVERAGE MAGNITUDE OF (k) IN MID-AXIAL PLANE AND AT 0.1D, 10D, AND 20D PLANES FROM THE NOZZLE OUTLET

sider LES or DNS for these types of simulations in the future.

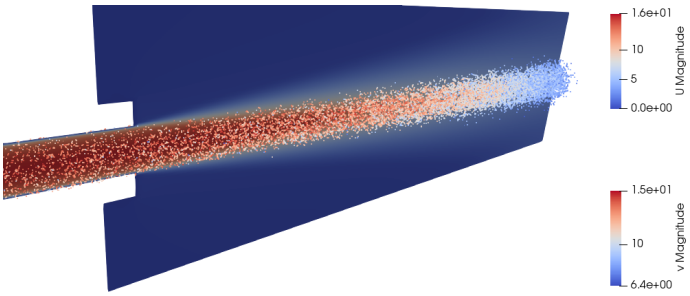

FIGURE 9. PARTICLES ISO VIEW

Figure 10 shows the average particle velocities as they are leaving the jet. It can be seen that particle velocities are at the greatest towards the outer regions of the jet. This is also observed in the experimental data given in Hardalupas et al. [4] and Lau et al. [28].

CONCLUSION

The coupled CFD-DEM numerical results at 10D and 20D from the nozzle outlet agree well with the experimental data for the mass loading of 0.23 and 0.86. However, the particle mass flux profiles at 0.1D plane do not agree. With conflicting evidence found in literature, it is difficult to discern the source of the discrepancy, but it is suspected that the entry length and its effect on the concentration profiles for both the experiments and numerical results are the probable cause. CFD-DEM simulations of turbulent jet flow are highly dependent on the particle insertion velocities as well and, therefore, to further validate and expand the applicability of the CFD-DEM method to turbulent particle-laden jet flow, it is imperative that high quality quantitative data from a highly controlled environment is collected and used in the future. The divided void fraction model in CFDEM®coupling

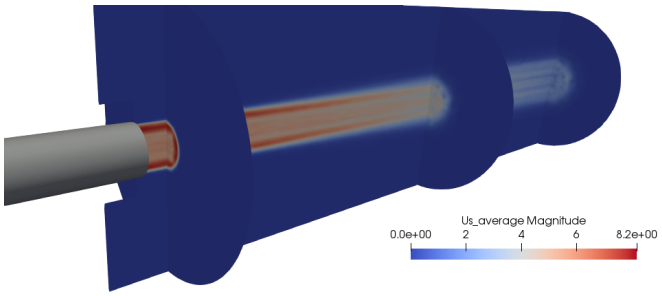

FIGURE 10. SMOOTHED AND AVERAGED PARTICLE VELOCITIES IN MID-AXIAL PLANE AND AT 0.1D, 10D, AND 20D PLANES FROM THE NOZZLE OUTLET

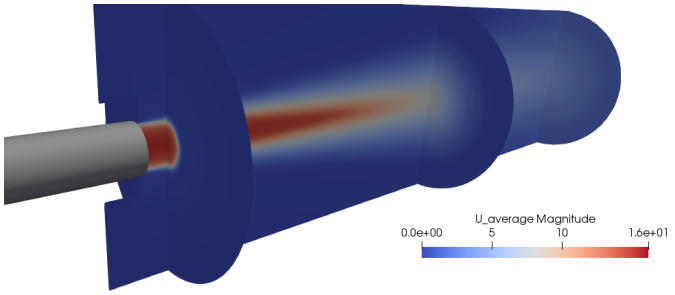

FIGURE 11. AVERAGE FLUID VELOCITIES IN MID-AXIAL PLANE AND AT 0.1D, 10D, AND 20D PLANES FROM THE NOZZLE OUTLET

provides consistent results for a mesh resolution of up to 1.86 particle diameters for dense turbulent jet flow.

ACKNOWLEDGMENT

The authors would like to acknowledge Compute Canada, West Grid and the University of British Columbia, Advanced Research Computing center (UBC ARC) for providing their support in the form of computational resources and technical help.

REFERENCES

[1] McComb, W., and Salih, S., 1977. "Measurement of normalised radial concentration profiles in a turbulent aerosol jet, using a laser-doppler anemometer". *Journal of Aerosol Science,* ***8***(3), June, pp. 171–181.

[2] McComb, W., and Salih, S., 1978. "Comparison of some theoretical concentration profiles for solid particles in a turbulent jet with the results of measurements using a laser-doppler anemometer". *Journal of Aerosol Science,* ***9***(4), Jan., pp. 299–313.

[3] Popper, J., Abuaf, N., and Hetsroni, G., 1974. "Velocity measurements in a two-phase turbulent jet". *International Journal of Multiphase Flow,* ***1***(5), Nov., pp. 715–726.

[4] Hardalupas, Y., Taylor, A., and Whitelaw, J., 1989. "Velocity and particle-flux characteristics of turbulent particle-laden jets". *Proceedings of the Royal Society of London. A. Mathematical and Physical Sciences,* ***426***(1870), Nov., pp. 31–78.

[5] Modarress, D., Tan, H., and Elghobashi, S., 1984. "Two-component LDA measurement in a two-phase turbulent jet". *AIAA Journal,* ***22***(5), May, pp. 624–630.

[6] Modarress, D., Wuerer, J., and Elghobashi, S., 1984. "AN EXPERIMENTAL STUDY OF A TURBULENT ROUND TWO-PHASE JET". *Chemical Engineering Communications,* ***28***(4-6), July, pp. 341–354.

[7] SHUEN, J.-S., 1984. "A Theoretical and Experimental Investigation of Dilute Particle-Laden Turbulent Gas Jets (two-Phase Flow)". Ph.D., The Pennsylvania State University, United States – Pennsylvania.

[8] Levy, Y., and Lockwood, F. C., 1981. "Velocity measurements in a particle laden turbulent free jet". *Combustion and Flame,* ***40***, pp. 333 – 339.

[9] Fairweather, M., and Hurn, J.-P., 2008. "Validation of an anisotropic model of turbulent flows containing dispersed solid particles applied to gas–solid jets". *Computers & Chemical Engineering,* ***32***(3), Mar., pp. 590–599.

[10] Kloss, C., Goniva, C., Hager, A., Amberger, S., and Pirker, S., 2012. "Models, algorithms and validation for open-source DEM and CFD-DEM". *Progress in Computational Fluid Dynamics, An International Journal,* ***12***(2/3), p. 140.

[11] Lorenz, A., Tuozzolo, C., and Louge, M. Y., 1997. "Measurements of impact properties of small, nearly spherical particles". *Experimental Mechanics,* ***37***(3), Sept., pp. 292–298.

[12] Norouzi, H., Zarghami, R., and Mostoufi, N., 2017. "New hybrid CPU-GPU solver for CFD-DEM simulation of fluidized beds". *Powder Technology,* ***316***, July, pp. 233–244.

[13] *voidfractionModel_dividedVoidFraction command — CFDEMcoupling v3.X documentation*.

[14] *OpenFOAM*.

[15] Menter, F. R., Kuntz, M., and Langtry, R. "Ten Years of Industrial Experience with the SST Turbulence Model". *Heat and Mass Transfer*, p. 8.

[16] Spalding, D. B., 1961. "A Single Formula for the "Law of the Wall"". *Journal of Applied Mechanics,* ***28***(3), Sept., pp. 455–458.

[17] Koch, D. L., and Hill, R. J., 2001. "INERTIAL EFFECTS IN SUSPENSION AND POROUS-MEDIA FLOWS". *Annual Review of Fluid Mechanics,* ***33***(1), Jan., pp. 619–647.

[18] van Buijtenen, M. S., van Dijk, W.-J., Deen, N. G., Kuipers, J., Leadbeater, T., and Parker, D., 2011. "Numerical and experimental study on multiple-spout fluidized beds". *Chemical Engineering Science,* ***66***(11), June, pp. 2368–2376.

[19] Issa, R., 1986. "Solution of the implicitly discretised fluid flow equations by operator-splitting". *Journal of Computational Physics,* ***62***(1), Jan., pp. 40–65.

[20] *LIGGGHTS Open Source Discrete Element Method Particle Simulation Code \textbar CFDEM®project*.

[21] Otsubo, M., O'Sullivan, C., and Shire, T., 2017. "Empirical assessment of the critical time increment in explicit particulate discrete element method simulations". *Computers and Geotechnics,* ***86***, June, pp. 67–79.

[22] Shokri, R., Ghaemi, S., Nobes, D., and Sanders, R., 2017. "Investigation of particle-laden turbulent pipe flow at high-Reynolds-number using particle image/tracking velocimetry (PIV/PTV)". *International Journal of Multiphase Flow,* ***89***, Mar., pp. 136–149.

[23] Varaksin, A. Y., Polezhaev, Y. V., and Polyakov, A. F., 2000. "Eect of particle concentration on uctuating velocity of the disperse phase for turbulent pipe ow". p. 6.

[24] Hosokawa, S., and Tomiyama, A., 2004. "Turbulence modification in gas–liquid and solid–liquid dispersed two-phase pipe flows". *International Journal of Heat and Fluid Flow,* ***25***(3), June, pp. 489–498.

[25] Karimi, S., Shirazi, S. A., and McLaury, B. S., 2017. "Predicting fine particle erosion utilizing computational fluid dynamics". *Wear,* ***376-377***, Apr., pp. 1130–1137.

[26] Gillies, R. G., Shook, C. A., and Xu, J., 2008. "Modelling Heterogeneous Slurry Flows at High Velocities". *The Canadian Journal of Chemical Engineering,* ***82***(5), May, pp. 1060–1065.

[27] Oliveira, J., van der Geld, C., and Kuerten, J., 2015. "Lagrangian velocity and acceleration statistics of fluid and inertial particles measured in pipe flow with 3D particle tracking velocimetry". *International Journal of Multiphase Flow,* ***73***, July, pp. 97–107.

[28] Lau, T. C. W., and Nathan, G. J., 2016. "The effect of Stokes number on particle velocity and concentration distributions in a well-characterised, turbulent, co-flowing two-phase jet". *Journal of Fluid Mechanics,* ***809***, Dec., pp. 72–110.